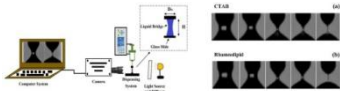
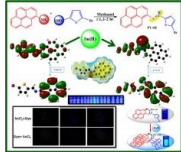


Sl. No.	<p style="text-align: center;"><b>IIT Ropar</b>  <b>List of Recent Publications with Abstract</b>  <b>Coverage: November, 2022</b></p>
1.	<p><a href="#">A detailed and systematic study on rheological and physicochemical properties of rhamnolipid biosurfactant solutions</a>  MB Khan, C Sasmal - JCIS Open, 2022</p> <p><b>Abstract:</b> Biosurfactants are widely used in many industrial settings ranging from cosmetic to petroleum industries. Among various biosurfactants available in the market, rhamnolipid is a well-known bacterial biosurfactant produced by the <i>Pseudomonas aeruginosa</i> bacteria. However, despite its wide applications, no detailed and systematic study is available on the rheological characterization of this biosurfactant solution, which is an essential property to investigate for many practical applications. Therefore, this study aims to present a thorough and complete investigation of this biosurfactant's shear and extensional rheological behaviours. While steady shear and small amplitude oscillatory shear (SAOS) measurements were conducted to investigate the shear rheological behaviour, the dripping-onto-substrate (DoS) extensional rheometry technique was used to understand its extensional rheological behaviour. A chemically derived surfactant (cetyltrimethyl ammonium bromide (CTAB)) was also used in our analysis to show and discuss the qualitative and quantitative differences in their rheological behaviours. Along with the detailed rheological study, some studies on the physicochemical properties, such as surface tension, contact angle, particle size analysis, thermal stability, etc., were also conducted to make an overall comparison between the two surfactants. Both surfactants show strong shear-thinning and extensional hardening behaviors in shear and extensional rheological flows, respectively. However, the zero-shear rate viscosity and extensional viscosity are found to be larger for rhamnolipid surfactant solutions than for CTAB. The corresponding shear and extensional relaxation times also follow the same trend. Furthermore, the surface tension is found to be less, and the contact angle is found to be more for rhamnolipid biosurfactant than that for CTAB. Rhamnolipid shows more excellent thermal stability, particularly at high temperatures than CTAB. Therefore, the results and discussion presented in this study will help to choose the present rhamnolipid biosurfactant for any particular application, particularly where the knowledge of the rheological responses of a surfactant solution is essential.</p> <p><b>Graphical abstract:</b></p>  <p>The graphical abstract illustrates the experimental setup and rheological data. On the left, a schematic shows a computer connected to a rheometer, which is linked to a syringe pump and a syringe. The syringe is used to perform dripping-onto-substrate (DoS) extensional rheometry. On the right, two sets of images show the droplet deformation during the DoS test. The top set, labeled 'CTAB', shows a droplet that deforms and then retracts. The bottom set, labeled 'Rhamnolipid', shows a droplet that deforms and then spreads, indicating higher extensional viscosity.</p>
2.	<p><a href="#">A hybrid-combine-and-forward relaying scheme for network coded cooperative systems</a>  S Bhattacharyya, P Kumar, S Sharma, S Darshi, AA Almohammed - IEEE International Conference on Advanced Networks and Telecommunications Systems (ANTS), 2022</p> <p><b>Abstract:</b> Network Coded Cooperation (NCC) proved itself worthy to meet the ever increasing demands of the next generation wireless users. In the prevalent relaying schemes, the relay either uses Amplify-and-Forward (AF) or Decode-and-Forward (DF) rigidly over all the signals received. However, some networks use Adaptive Decode-Forward (ADF) where relay only forwards the decoded data which causes resource wastage as the sources need to re-transmit the data which were not sent by the relay. This paper proposes a Hybrid-Combine-and-Forward (HCF) relaying scheme for a multi-user scenario to improve the Quality-of-Support (QoS) in a cost effective manner. With the HCF scheme, the relay dynamically performs AF on some of the received signals while DF on the rest, and stores them within a communication cycle. This decision is taken by the relay based on the Instantaneous Signal-to-Noise Ratio (SNR<sub>i</sub>) of the</p>

	<p>signal received from the respective sources. Finally, it combines all the stored signals received and transmits a hybrid superposed data to the destinations which is required to extract the second copy of the desired data. Extensive simulations provide results showing the superiority of the proposed HCF scheme over the widely used AF and DF schemes. Such a scheme can be used in a Device-to-Device (D2D) communication/ Vehicle-to-Everything (V2X) networks or in scenarios like disaster management where sources aided by a drone/relay require reliable data at a low operational cost of the relay.</p>
3.	<p><a href="#">A miniaturized dual-resonator-based high-capacity chipless radio frequency identification tag sensor</a>  SK Gupta, S Kumar, A Sharma - IEEE Sensors Letters, 2022</p> <p><b>Abstract:</b> The chipless radio-frequency identification (RFID) sensor is a potential technology for future RFID-based sensing systems. A novel ultra-wideband and retransmission-method-based frequency-coded chipless RFID tag is presented in this letter. The footprint of the proposed RFID tag is reduced by incorporating spur-line spiral resonators along with the spiral resonators. These resonators are designed within and around the transmission line connecting two orthogonal ports of the dual-polarized monopole antenna operating in the transceiver mode. Initially, the patch antenna and the resonator circuits are optimized separately for the intended impedance bandwidth and frequency response, respectively, and are later integrated together to achieve the required performance. The operating range of the tag antenna is from 2 to 5.2 GHz. Furthermore, two prototypes of the proposed RFID tag with the 10-b code are fabricated and tested. The simulation and experimental results are found to be in good agreement, validating the proposed design.</p>
4.	<p><a href="#">A new strategy of defect passivation in kesterite absorber layer to engineer the band tailing for efficient carrier transport</a>  Nisika, A Ghosh, K Kaur, MK Yadav, A Bag, M Kumar - Applied Physics A, 2022</p> <p><b>Abstract:</b> <math>\text{Cu}_2\text{ZnSnS}_4</math> (CZTS) absorber materials are often associated with high non-radiative recombination and band tailing which results in poor material properties. Herein, we successfully employ a small molecule, triethanolamine, to passivate the charged point defects and dangling bonds not only on the CZTS surface but also within the CZTS absorber. The Urbach energy of treated CZTS absorber reduced by 0.29 eV besides increased bandgap value unraveled the passivation of band-edge tail states. The band-to-band transitions (<math>\sim 6</math> times) enhanced over band-to-tail transitions in PL spectra after the treatment representing the significant suppression of non-radiative recombination. Our studies reveal that due to passivation of CZTS surface, the interface trap density was substantially reduced, influencing charge carrier dynamics of CZTS/<math>\text{TiO}_2</math> heterojunction-based devices. This work provides an insight toward the unexplored direction of chemical treatment of CZTS absorber to modulate its optical and electrical properties.</p>
5.	<p><a href="#">A non-linear time series based artificial intelligence model to predict outcome in cardiac surgery</a>  S Konar, N Auluck, R Ganesan, AK Goyal, T Kaur, M Sahi... - Health and Technology, 2022</p> <p><b>Abstract:</b></p> <p>Background</p> <p>Adverse lifestyles have led to increased cardiac complications, further accelerating the burden of cardiac surgeries in tertiary care hospitals. For optimum management of cardiac surgical patients in the hospital, it is essential to have an accurate idea regarding the patients' expected ICU stay and hospital stay. Additionally, forecasting patients' survival outcome is also essential for ICU management.</p> <p>Objectives</p>

	<p>This study aims to develop artificial intelligence models based on non-linear time-series data of blood pressure and heart rate to predict the ICU stay, hospital stay, and survival outcome of cardiac surgical patients.</p> <p><b>Methods</b> The intraoperative heart rate and blood pressure data of 6064 patients undergoing cardiac surgeries at a single tertiary care hospital were recorded every minute. After data cleaning, the data was split into 781 patients in the train data set and 296 patients in the test data set. Feature engineering and balancing of data were performed on the train data set. Various classification models for survival outcome and regression models for ICU stay and hospital stay were trained using the balanced train data set. These models were tested on the test data set, and the prediction results were evaluated on the following performance metrics: area under the curve (AUC), accuracy, F1-score, RMSE, and R2-score.</p> <p><b>Results</b> The Gaussian Naive Bayes + Logistic Regression (GNB + LR) model is the best for survival analysis, having the highest AUC of 0.72, Accuracy of 83%, and an F1-score of 0.86. The Gradient boosting (GB) model is the best model for the analysis of hospital stay, offering the highest R2-score (0.023). The XGBoost regressor is the best model for ICU stay analysis, offering the highest R2-score (0.125).</p> <p><b>Conclusion</b> Artificial intelligence models based upon the intraoperative time series data were developed to analyse outcomes in cardiac surgery with high accuracy. These models can be used in cardiac surgeries to predict the ICU stay, hospital stay, and overall survival of the patients for better ICU management at the hospital.</p>
6.	<p><a href="#">A novel power consumption optimization framework in 5G heterogeneous networks</a> K Venkateswararao, P Swain, SS Jha, I Ioannou... - Computer Networks, 2022</p> <p><b>Abstract:</b> The fifth-generation (5G) mobile networks have the capacity to handle the dynamic traffic demands of the user equipment (UE). One approach is the dense deployment of small base stations (s-BSs), which can control the dynamic traffic demands. We consider s-BSs which are interconnected through the mmWave backhaul (BH) link to transfer traffic from the s-BS to the core network through the macro base station (MBS). In this setting, the network power consumption is affected by the way UEs are connected to the base stations and the traffic routes through the BH links. The main objective of this paper is to minimise the power consumption of the heterogeneous network (HetNet) with the intelligent backhauling and s-BS/BH link sleeping (IBSBS) framework. The proposed framework provides the minimised power consumption in HetNets through UE association, backhauling, and sleep s-BS/BH links. The UE association and backhauling uses a heuristic function based intelligent backhauling algorithm to assess the minimum power consumption from the s-BS to the MBS while considering the power and capacity constraints of the network. The load sharing based s-BS sleeping algorithm dynamically changes the states (active/sleep) of the s-BSs according to their loads without compromising UE demands. Different distributions of UEs and different data rates over the HetNets architecture are considered for performance evaluation. The evaluation results of the proposed framework outperform the state-of-the-art algorithms in terms of network energy efficiency, power consumption, and the number of active s-BSs/BH links.</p>
7.	<p><a href="#">A novel pyrene-based aggregation induced enhanced emission active Schiff base fluorophore as a selective “turn-on” sensor for Sn<sup>2+</sup> ions and its application in lung adenocarcinoma cells</a> VS Rana, V Anand, SS Sarkar, N Sandhu, M Verma, S Naidu... - Journal of Photochemistry and Photobiology A: Chemistry, 2022</p>

	<p><b>Abstract:</b> Schiff bases are an important class of compounds that are highly instrumental in complex formation as well as act as sensors for various metal ions. Herein, 1-aminopyrene was reacted with 5-bromo-2-thiophene carboxaldehyde to synthesize a designed Schiff base, <b>PY-SB</b> (N-((5-bromothiophen-2-yl) methylene) pyrene-2-amine) as a condensation product. The authenticity of the synthesized Schiff base compound was established using <math>^1\text{H}</math> NMR, <math>^{13}\text{C}</math> NMR, IR and HRMS techniques. Among the optoelectronic investigations, the AIEE (Aggregation Induced enhanced emission) property of PY-SB was explored and it showed 24 folds enhancement in fluorescence intensity in tetrahydrofuran (THF) and water mixtures (50:50). AIEE results were further supported by DLS (Dynamic Light scattering) study. In addition, <b>PY-SB</b> was found to be a highly selective and sensitive tool for the “turn-on” detection of <math>\text{Sn}^{2+}</math> ion. The turn-on fluorescence of PY-SB is due to the PET-OFF process. The electron transfer from nitrogen to the pyrene ring is completely blocked due to the formation of a complex of PY-SB with insitu generated <math>\text{Sn}^{2+}</math> species (<math>\text{PY-SB} + \text{Sn}^{2+}</math>), which causes PET-OFF. The detection limit and binding constant of <b>PY-SB</b> towards <math>\text{Sn}^{2+}</math> ion were found to be <math>5.4\ \mu\text{M}</math>, and <math>2 \times 10^4\ \text{M}^{-1}</math>, respectively. The stoichiometric study through Job’s plot reveals the development of 2:1 ratio (<math>\text{Sn}^{2+}</math>: PY-SB) of complexation which is further confirmed by DFT, ES-MS, <math>^1\text{H}</math> NMR and <math>^{13}\text{C}</math> NMR, SEM-EDX. To verify the sensing behavior of <b>PY-SB</b> in a biological system, in vitro studies on lung adenocarcinoma cells were successfully carried out and they showed similar behavior as seen in the cuvette study.</p> <p><b>Graphical abstract:</b></p> 
8.	<p><a href="#">A planar orbicular rectenna array system with 3-D uniform coverage for wireless powering of IoT nodes</a>  M Kumar, S Kumar, A Sharma - IEEE Transactions on Microwave Theory and Techniques, 2022</p> <p><b>Abstract:</b> Microwave power transfer (MPT) is a revolutionary technique for charging batteries of wireless sensor nodes in smart applications. However, sensor nodes can be positioned at any arbitrary orientation and location with respect to the microwave transmitter (Tx). Therefore, harvested DC power depends on the node’s position and orientation. Thus, to reduce this reliance, a novel, fully integrated planar multisector rectenna (Rx) array is designed to achieve a nearly uniform 3-D spherical DC coverage. To realize orientation insensitive azimuth and elevation plane coverage, the proposed Rx features eight radially arranged endfire Rx (EFR-antenna) elements, and a bore-sight Rx (BSR-antenna) element with multiarms for inherent DC combining is used at the center with orthogonally polarized ports. Furthermore, direct conjugate matching of antenna and rectifier circuit with integrated operation is applied to realize a fully integrated design. This reduces insertion losses and achieves the desired 3-D coverage along with miniaturization, shaping it suitable for deployment at space-constrained IoT sensor nodes for orientation oblivious wireless powering.</p>
9.	<p><a href="#">A switched modular multi-coil array transmitter pad with coil rectenna sensors to improve lateral misalignment tolerance in wireless power charging of drone systems</a>  A Bharadwaj, A Sharma, CR Chandupatla - IEEE Transactions on Intelligent Transportation Systems, 2022</p> <p><b>Abstract:</b> In this article, a Switched Modular Multi-coil Array transmitter pad integrated with coil RecTenna (SMMART) is designed to present an intelligent wireless drone charging system</p>

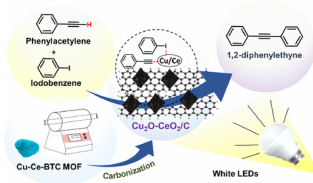
	<p>that improves lateral misalignment tolerance. The resultant optimized design constitutes four independent transmitter modules, wherein each includes four spatially distributed 2×2 array coils. Therefore, the proposed design induces a maximal uniform voltage in the Rx coil region. Moreover, the optimization procedure accounts for the miniaturization of transmitter coil size without compromising the misalignment tolerance by overlapping various transmitter modules. In addition, a novel coil-based detection system for wireless chargeable drone applications is proposed to activate the desired transmitter module based on the position of the receiver coil. The detection system consists of an array of coil rectennas integrated with a switching circuit to reduce the undesired magnetic field, enhancing the link efficiency. The prototype of the charging pad is fabricated using Litz wire, and the S21-based link efficiency is measured using an experimental setup. Besides, the fabricated coil rectenna sensor array system demonstrates a real-application model of the detection system. Hence, the proposed transmitter pad improves lateral misalignment tolerance and is considered a potential wireless drone charging system design.</p>
10.	<p><a href="#">A theoretical framework to analyse the flow of particles in a dynamical system with stochastic transition rates and site capacities</a>  A Jain, A Kumar, AK Gupta - Royal Society Open Science, 2022</p> <p><b>Abstract:</b> We study the stochasticity in a dynamical model: ribosome flow model with different site sizes that models the unidirectional movement of particles controlled by transition rates along a lattice having different site sizes. Our work models the parameters as random variables with known distributions and investigates the steady-state flow rate under this notion by using tools from the random matrix theory. Some closed-form theoretical results are derived for the steady-state flow rate under some restrictive assumptions such as random variables being independent and identically distributed. Furthermore, for arbitrary but bounded stochastic transition rates, stochastic site capacities, or both, we establish bounds for the steady-state flow rate. Our analysis can be generalized and applied to study the flow of particles in numerous transport systems in the stochastic environment.</p>
11.	<p><a href="#">Algebraic Method for Approximate Solution of Scattering of Surface Waves by Thin Vertical Barrier Over a Stepped Bottom Topography</a>  N Kumar, D Goyal, SC Martha - Contemporary Mathematics, 2022</p> <p><b>Abstract:</b> A study on interaction of surface water waves by thin vertical rigid barrier over a step type bottom topography is analysed. The associated mixed boundary value problem is solved using the eigenfunction expansion of the velocity potential. The resulting system of equations, avoiding the traditional approach of employing application of orthogonality relations, is solved using algebraic least squares method giving rise the numerical values of the reflection and transmission coefficients by the barrier over step. The energy balance relation for the given problem is derived and verified numerically ensuring the correctness of the present results. The present results are also compared with the data available in the literature for the validation purpose. The effect of step height, length of the barrier and angle of incidence on the reflection coefficient and the non-dimensional horizontal force on the barrier have been investigated through different plots. It is observed that barrier along with step works as an effective barrier to reflect more incident waves causing calm zone along the leeside.</p>
12.	<p><a href="#">An Experimental Study of the Concept Drift Challenge in Farm Intrusion Detection using Audio</a>  R Bhatt, S Singh, P Choudhary, M Saini - IEEE International Conference on Advanced Video and Signal Based Surveillance (AVSS), 2022</p> <p><b>Abstract:</b> Intrusion detection in farm settings is a challenging task. The data distribution suffers significant drift due to variations in environmental sounds. In this paper, we study the effect of this drift on state-of-the-art deep models. We experimentally found that the traditional models fail to deal with such variations and exhibit performance degradation. VGG16 turns out to be the best deep model, which shows an improvement of 2.76% over the best-performing state-of-the-</p>



	<p>art deep model on parameter F1-score. Consequently, we make an initial attempt to overcome this drift by integrating an unsupervised background noise component with standard models. On denoised signals, we obtained an average improvement of 50% on parameter accuracy for VGG16. The experimental analysis demonstrates the need for adaptive learning to handle the Spatio-temporal drifts in outdoor farm settings.</p>
13.	<p><a href="#">Assessment of Mitochondrial Health in Cancer-Associated Fibroblasts Isolated from 3D Multicellular Lung Tumor Spheroids</a>  L Arora, M Kalia, S Roy, D Pal - Journal of Visualized Experiments: Jove, 2022</p> <p><b>Abstract:</b> Cancer-associated fibroblasts (CAFs) are among the most abundant stromal cells present in the tumor microenvironment, facilitating tumor growth and progression. Complexity within the tumor microenvironment, including tumor secretome, low-grade inflammation, hypoxia, and redox imbalance, fosters heterotypic interaction and allows the transformation of inactive resident fibroblasts to become active CAFs. CAFs are metabolically distinguished from normal fibroblasts (NFs) as they are more glycolytically active, produce higher levels of reactive oxygen species (ROS), and overexpress lactate exporter MCT-4, leading to the opening of the mitochondrial permeability transition pore (MPTP). Here a method has been described to analyze the mitochondrial health of activated CAFs isolated from the multicellular 3D tumor spheroids comprising of human lung adenocarcinoma cells (A549), human monocytes (THP-1), and human lung fibroblast cells (MRC5). Tumor spheroids were disintegrated at different time intervals and through magnetic-activated cell sorting, CAFs were isolated. The mitochondrial membrane potential of CAFs was assessed using JC-1 dye, ROS production by 2',7'-dichlorodihydrofluorescein diacetate (DCFDA) staining, and enzyme activity in the isolated CAFs. Analyzing the mitochondrial health of isolated CAFs provides a better understanding of the reverse Warburg effect and can also be applied to study the consequences of CAF mitochondrial changes, such as metabolic fluxes and the corresponding regulatory mechanisms on lung cancer heterogeneity. Thus, the present study advocates an understanding of tumor-stroma interactions on mitochondrial health. It would provide a platform to check mitochondrial-specific drug candidates for their efficacies against CAFs as potential therapeutics in the tumor microenvironment, thereby preventing CAF involvement in lung cancer progression.</p>
14.	<p><a href="#">Atlas of nuclear isomers—Second edition</a>  S Garg, B Maheshwari, B Singh, Y Sun, A Goel... - Atomic Data and Nuclear Data Tables, 2022</p> <p><b>Abstract:</b> We present an updated version of the 2015-Atlas of Nuclear Isomers (Jain et al., 2015), compiling and evaluating experimental data for the isomers with half-life <math>\geq 10</math> ns, together with their spectroscopic properties such as excitation-energies, half-lives, decay modes, spins and parities, energies and multipolarities of isomeric transitions, along with the relevant original references in literature. The current version of Atlas presents many re-evaluated half-lives as compared to the 2015 edition, where values were referred to Nuclear Data Sheets publications, when no new data existed. The ENSDF database (Burrows, 1990), together with the XUNDL (XUNDL database, <a href="http://www.nndc.bnl.gov/ensdf/ensdf/xundl.jsp">http://www.nndc.bnl.gov/ensdf/ensdf/xundl.jsp</a>) and the NUBASE2020 (Kondev et al., 2021) databases have been consulted for completeness, yet, data from original papers from journals were considered in the present evaluation, and the NSR bibliographic database (Pritychenko et al., 2011) has been searched to ensure that this work is as complete and current as possible. Several useful systematic features of nuclear isomers covered in this Atlas have been discussed. Literature cutoff date for the extraction of data is October 31, 2022.</p>
15.	<p><a href="#">Connectivity Improvement of Hybrid Millimeter Wave and Microwave Vehicular Networks</a>  D Saluja, R Singh, N Saluja, S Kumar - IEEE Transactions on Intelligent Transportation Systems, 2022</p> <p><b>Abstract:</b> The network connectivity while traveling in a vehicle is an important issue, which</p>

	<p>needs to be addressed by mobile vehicular networks. This paper proposes a novel scheme to improve the connectivity of mobile vehicular networks. In particular, the paper proposes a medium access control (MAC) layer hybrid mmWave and microwave scheme for vehicular networks, and leverage their capabilities to improve the vehicle's connectivity. The novel computational model is derived to evaluate the connectivity for the proposed scheme. The model is used for performance analysis of vehicles moving on a multi-lane highway road and getting connectivity with road-side-units (RSUs) deployed along the roads. Our analysis considers that reference VN has perfect channel state information. It is assumed that the RSU radiates ubiquitously on the road surface using microwave radio access technology (RAT), while it radiates directionally towards reference VN using mmWave RAT. For mathematical analysis, the directionality in mmWave RAT is well approximated by a sectorized antenna model. The analysis for the proposed scheme is compared with the existing mmWave network and packet data convergence protocol (PDCP) layer hybrid scheme. The analysis claims that the proposed hybrid scheme significantly improves the connectivity performance in mobile vehicular networks over the existing schemes. The computation results are validated with the simulation results. Also, the paper offers parametric analysis for connectivity probability with vehicle speed and slot duration to enable its practical implementation in 5G/6G technologies.</p>
16.	<p><a href="#"><u>Consolidated Adversarial Network for Video De-raining and De-hazing</u></a>  VM Galshetwar, A Kulkarni, S Chaudhary - IEEE International Conference on Advanced Video and Signal Based Surveillance (AVSS), 2022</p> <p><b>Abstract:</b> The performance of recent video enhancement methods is superior in specific hazy, rainy, snowy, and foggy weather conditions. However, these approaches can handle degradation rendered by single weather. We propose an integrated lightweight adversarial learning network to handle the degradations induced by different weather conditions. This is a unique approach to mitigate the problem of video restoration for multi- weather degraded videos using single network. The proposed architecture combines the idea of multi-resolution analysis with a multi-scale encoder and domain-specific feature learning is achieved using domain-aware filtering modules. The architecture provides recurrent feature sharing for temporal consistency, achieved by feeding the previous frame output as feedback. Substantial experiments on various datasets demonstrate that the proposed method performs competitively with the existing state-of-the-art approaches for video restoration in multi-weather conditions.</p>
17.	<p><a href="#"><u>Cu–Ce Bimetallic Metal–Organic Framework-Derived, Oxygen Vacancy-Boosted Visible Light-Active Cu<sub>2</sub>O–CeO<sub>2</sub>/C Heterojunction: An Efficient Photocatalyst for the Sonogashira Coupling Reaction</u></a>  GS More, AK Kar, R Srivastava - Inorganic Chemistry, 2022</p> <p><b>Abstract:</b> The development of an economical transition metal-based catalyst for photocatalytic carbon–carbon coupling reactions is aspiring. Herein, a Cu–Ce metal–organic framework (MOF) was synthesized and carbonized to produce bimetallic Cu<sub>2</sub>O–CeO<sub>2</sub>/C, which was utilized in the Sonogashira cross-coupling reaction. The defects and oxygen vacancies in the catalyst were characterized by X-ray photoelectron spectroscopy and Raman spectroscopy, while the nature of Cu was characterized by H<sub>2</sub>-TPR analysis. The defect-induced MOF-derived Cu–Ce heterojunction created more oxygen vacancies (O<sub>v</sub>) in CeO<sub>2</sub>, revealing the high photocatalytic activity. The Cu–Ce heterojunction (Cu<sub>2</sub>O–CeO<sub>2</sub>/C) formed a Cu(I)–phenylacetylide active complex and exhibited higher catalytic activity for the visible light-induced Sonogashira cross-coupling reaction. 25% Cu<sub>2</sub>O–CeO<sub>2</sub>/C offered 93.8% phenylacetylene conversion with a 94.2% Sonogashira product selectivity by using household light-emitting diodes. No discernible activity loss was observed from the recycling of the catalyst. Based on catalytic activity, control reactions, and physicochemical and optoelectronic characterization, the structure–activity relationship was established and a reaction mechanism was proposed. Replacement of the costly Pd metal-based catalyst with a cheap Cu<sub>2</sub>O–CeO<sub>2</sub>-based catalyst for the synthesis of</p>

commercially important compounds with a sustainable visible light-induced catalytic process will be highly attractive to chemists and industrialists.



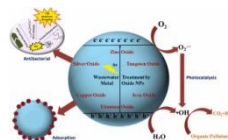
[Current developments in nanostructurally engineered metal oxide for removal of contaminants in water](#)

S Singh, R Garg, A Jana, C Bathula, S Naik, M Mittal - *Ceramics International*, 2022

18.

**Abstract:** Clean water is one of the vital resources of every living being residing on this earth. However, rapid industrialization, growing human population, urbanization, global warming, extensive agricultural practices, and climatic change have deprived them of access to clean water. These factors convert clean water into wastewater by polluting water and making it poisonous due to heavy metals. 3.575 million deaths are observed from diseases caused by waste or polluted water every year, according to the World Health Organization report. Hence, wastewater treatment has become every country's primary concern. Although several conventional methods are available for wastewater treatment, their utilization has been restrained due to the high maintenance cost of equipment, the large surface area for installation, and a large amount of energy. Nanotechnology offers a lot of potential for improving the efficiency of water purification and disinfection. Nanomaterials can remove inorganic and organic pollutants, biological pollutants (fungi, bacteria, and microbes), and heavy metal ions from wastewater. Metal oxide nanoparticles (NPs) are the most diverse class of materials due to their unique properties such as good adsorption capacity, large surface area, improved catalysis, and enhanced reactivity. Hence, metal oxide NPs have applications in wastewater treatment. A comprehensive overview of the numerous metal oxide NPs in wastewater treatment has been presented in this review. Here, in detail, we have discussed zinc oxide, titanium oxide, silver oxide, tungsten oxide, iron oxide, and copper oxide NPs and their application in wastewater treatment.

**Graphical abstract:**



[Deep Network for Extremely Low-Resolution Human Action Recognition](#)

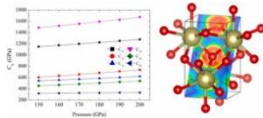
S Chaudhary, PW Patil, A Dudhane, S Murala - *IEEE International Conference on Advanced Video and Signal Based Surveillance (AVSS)*, 2022

19.

**Abstract:** Due to advancement in automated applications, privacy-preserving is an emerging concern. This concern is more significant in the case of human-centred surveillance application like human action recognition (HAR). Along with privacy concern, the computational complexity due to the huge size of video data is another major concern. To overcome these limitations, an attempt is made to examine the domain of human action recognition in low-resolution (LR) videos. The extremely LR video data ensures sufficient distortion in visual information to hide the identity of the person. Therefore, working with LR videos can resolve the above mentioned concerns of privacy preserving and computational complexity up to a certain



	<p>extent. In this paper, a new generative adversarial network (GAN) based neural architecture is proposed for HAR in extremely low-resolution videos. The extensive results analysis with ablation study on the state-of-the-art datasets proves the effectiveness of the proposed method over the existing methods for LR-HAR.</p>
20.	<p><a href="#">DeepDeMod: BPSK Demodulation Using Deep Learning Over Software-Defined Radio</a> A Ahmad, S Agarwal, S Darshi, S Chakravarty - IEEE Access, 2022</p> <p><b>Abstract:</b> In wireless communication, signal demodulation under non-ideal conditions is one of the important research topic. In this paper, a novel non-coherent binary phase shift keying demodulator based on deep neural network, namely DeepDeMod, is proposed. The proposed scheme makes use of neural network to decode the symbols from the received sampled signal. The proposed scheme is developed to demodulate signal under fading channel with additive white Gaussian noise along with hardware imperfections, such as phase and frequency offset. The time varying nature of hardware imperfections and channel poses a additional challenge in signal demodulation. In order to address this issue, additionally we propose transfer learning based DeepDeMod scheme. Pilot symbols along with data is transmitted in a packet which is used to learn the time varying parameters from the pilot reception followed by data demodulation. Results show that compared with the conventional demodulators and other machine learning based demodulators, our proposed DeepDeMod provides significantly better performance in term of bit error rate. We also implement the proposed DeepDeMod on software defined radio and present the experimental results.</p>
21.	<p><a href="#">Discovery of oxindole-based FLT3 inhibitors as a promising therapeutic lead for acute myeloid leukemia carrying the oncogenic ITD mutation</a> O Bender, ME Shoman, TFS Ali...JA Malik... - Archiv der Pharmazie, 2022</p> <p><b>Abstract:</b> FMS-like tyrosine kinase 3 (FLT3) mutations occur in approximately 30% of acute myeloid leukemia (AML) patients. In the current study, the oxindole chemotype is employed as a structural motif for the design of new FLT3 inhibitors as potential hits for AML irradiation. Cell-based screening was performed with 18 oxindole derivatives and <b>5a–c</b> inhibited 68%–73% and 83%–91% of internal tandem duplication (ITD)-mutated MV4-11 cell growth for 48- and 72-h treatments while only 0%–2% and 27%–39% in wild-type THP-1 cells. The most potent compound <b>5a</b> inhibited MV4-11 cells with IC<sub>50</sub> of 4.3 µM at 72 h while it was 8.7 µM in THP-1 cells, thus showing two-fold selective inhibition against the oncogenic ITD mutation. The ability of <b>5a</b> to modulate cell death was examined. High-throughput protein profiling revealed low levels of the growth factors IGFBP-2 and -4 with the blockage of various apoptotic inhibitors such as Survivin. p21 with cellular stress mechanisms was characterized by increased expression of HSP proteins along with TNF-β. Mechanistically, compounds <b>5a</b> and <b>5b</b> inhibited FLT3 kinase with IC<sub>50</sub> values of 2.49 and 1.45 µM, respectively. Theoretical docking studies supported the compounds' ability to bind to the FLT3 ATP binding site with the formation of highly stable complexes as evidenced by molecular dynamics simulations. The designed compounds also provide suitable drug candidates with no violation of drug likeability rules.</p>
22.	<p><a href="#">Effect of Hele–Shaw cell gap on radial viscous fingering</a> S Nand, V Sharma, SK Das, SS Padhee, M Mishra - Scientific Reports, 2022</p> <p><b>Abstract:</b> The flow through a Hele–Shaw cell is an experimental prototype to study the flow through a porous medium as well as the flow in microfluidic devices. In context with porous medium flows, it is used to visualize and understand hydrodynamic instabilities like viscous fingering (VF). The gap between the plates of the cell is an important parameter affecting the flow dynamics. However, the effect of the gap on the Hele–Shaw cell flows has been minimally explored. We perform experiments to understand the effect of the gap on VF dynamics. It is observed that a minimum gap is required to observe rigorous fingering instability. The onset time of instability, as well as the width of the fingers, increases with an increment in the gap due to a</p>

	<p>decrease in the convection. The instability increases with an increase in Péclet number, but the effect of gap width on fingering patterns is evident with broader fingers observed for larger <math>b</math>. The results are validated by performing numerical simulations. It is further shown that the gap-averaged three-dimensional simulations using the Stokes law approach and the two-dimensional Darcy's law result in a small gap Hele–Shaw cell.</p>
23.	<p><a href="#">Effectiveness of forced cooling during laser bending of duplex-2205</a>  R Yadav, R Kant - Materials and Manufacturing Processes, 2022</p> <p><b>Abstract:</b> Duplex-2205 is a dual-phase stainless steel having high mechanical strength and excellent corrosion resistance properties. Large spring back and high heat sensitivity are major problems in duplex-2205 during cold and hot working, respectively. Laser bending process is an advanced manufacturing process that is used for difficult to form materials with minimum heat-affected zone, negligible spring back, and high precision. Forced cooling (FC) has improved the efficiency during multiscan laser bending by reducing the waiting time. This study is focused on the analysis of the effectiveness of FC at the lower surface during single scan laser bending of duplex-2205 stainless steel. Worksheet geometry (thickness and width) and laser parameters (beam diameter, scanning speed and power) are varied to analyze the temperature profile, bend angle, mechanical and metallurgical properties during FC and compared with natural cooling condition. The results showed that a higher bend angle is observed in FC compared to natural cooling. Furthermore, tensile strength and hardness are improved whereas ductility is reduced due to change in phase distribution in the scanning region. Moreover, FC is found to be more effective at higher laser power, lower scanning speed, intermediate beam diameter, lower sheet thickness, and longer width of the worksheet.</p>
24.	<p><a href="#">Electronic topological transitions and mechanical properties of hafnium dioxide allotrope at high pressure: Evolutionary first-principles techniques</a>  T Bovornratanaraks, R Ahuja, W Luo... - Physica B: Condensed Matter, 2022</p> <p><b>Abstract:</b> Allotrope of <math>\text{HfO}_2</math> is explored by using first-principles evolutionary algorithm technique, based on density functional theory. The tetragonal structure with the space group of <math>P4/nmm</math> is demonstrated thermodynamically stable within the harmonic level. Arising particularly from the relative enthalpy, hafnium dioxide allotrope is taken into account in appraising the dynamic stability. Following this, the phonon calculations display that hafnium dioxide allotrope is dynamically stable under compressed conditions. Along with electronic properties, the band structure and density of states demonstrate that hafnium dioxide allotrope is semiconductor. Besides, the more significant change in the shape of density of states is observed when the increase in pressure, by adopting an effect of this electronic topological transition, resulting in the energy gap decreased monotonically. By inspecting their elastic constants and Vicker's hardness, the <math>P4/nmm</math> structure displayed the Vicker's hardness of 26.1 GPa at a pressure of 200 GPa. These findings suggest <math>\text{HfO}_2</math> is more likely to be attained experimentally and theoretically in metal oxides family.</p> <p><b>Graphical abstract:</b></p> 
25.	<p><a href="#">Estimation and validation of standalone SCATSAT-1 derived snow cover area using different MODIS products</a>  S Singh, RK Tiwari, V Sood, R Kaur, S Singh... - Geocarto International, 2022</p>

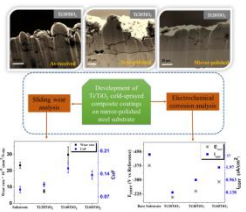
	<p><b>Abstract:</b> In the present work, the scatterometer satellite (SCATSAT-1) has been implemented and validated to provide the near-real-time estimation of snow cover area (SCA) in the Western Himalayas, India. The SCA derived from standalone SCATSAT-1 L4 (Level-4 India) products, i.e. sigma-nought (<math>\sigma^\circ\sigma^\circ</math>), and gamma-nought (<math>\gamma^\circ\gamma^\circ</math>) has been validated with different MODIS products individually, i.e. MOD02 L1B (calibrated-radiances) derived NDSI (normalized difference snow index), MOD10A1 L3 (daily composite snow cover), and MOD10A2 L3 (8-Day composite snow cover). The experimental outcomes confirm the potential of SCATSAT-1 in estimating the SCA with respect to other MODIS products and also, suggested the utilization of the different MODIS products for referencing/validation in different scenarios. The findings of this paper suggest that SCATSAT-1 offers the near real-time mapping and monitoring of large-scale snow extent at the global level even under cloudy conditions.</p>
26.	<p><a href="#"><u>Evaporation kinetics of wettability-moderated capillary bridges and squeezed droplets</u></a>  A Paul, D Samanta, P Dhar - Chemical Engineering Science, 2022</p> <p><b>Abstract:</b> We experimentally and theoretically probe the evaporation kinetics of liquid capillary bridges and squeezed droplets for different heights and wettability conditions. Water droplets of uniform volume were squeezed between hydrophilic and superhydrophobic (SH) flat substrates, and the relative spacing between them is varied to understand the role of bridge height on its evaporation behavior. The transient evolution of bridge profile during the evaporation is monitored using optical imaging technique, with thermal imaging aid. Our observations reveal augmented evaporation rate for smaller relative spacing between the hydrophilic surfaces due to increased curvature of the liquid–vapor interface. For SH surfaces, the vapor entrapment phenomenon plays a significant role in addition to interfacial curvature, especially for small relative spacing. For mixed wettability bridge, the shape of the bridge exhibits a transition in curvature, which governs its temporal evaporation rate. We show that the bridge stability and contact line dynamics during evaporation is strongly dictated by the capillary pressure and the geometry of the liquid–vapor interface. For smaller relative spacing, the contact line de-pins at early stages and the liquid bridge remains stable for a longer duration. Whereas, bridges pinch off at early stages for higher spacing conditions via rapid evaporation of the neck. To model the evaporative mass loss rate, the transient bridge interfacial profile under influence of gravity is quantified using the principal of energy minimization, and the curvature driven evaporative flux is summed up over this interface to obtain the evaporation rate. The model predictions conform well to the experimental observations.</p>
27.	<p><a href="#"><u>Exergy analysis and investigation on effect of inlet valve closing temperature and hydrogen enrichment in syngas composition in an HCCI engine</u></a>  MR Saxena, RK Maurya - International Journal of Hydrogen Energy, 2022</p> <p><b>Abstract:</b> This study presents the parametric investigation of syngas fuelled homogeneous charge compression ignition (HCCI) engine. The chemical kinetic simulation of the syngas HCCI engine is performed using the stochastic reactor model (SRM). This study first compares and evaluates the performance of different reaction mechanisms for the HCCI engine. The experimental combustion pressure data is compared with numerically investigated combustion pressure to validate the reaction mechanisms. Results indicate that a numerically simulated combustion pressure using a detailed reaction mechanism consisting of 173 reactions and 32 species (CRECK-2014) is well-matched with the profile of experimental combustion pressure. The validated reaction mechanism is further used to investigate the HCCI engine at different engine speeds for various equivalence ratio (<math>\phi</math>), syngas composition (hydrogen addition (<math>H_2:CO</math>)) and inlet valve closing temperature (<math>T_{ivc}</math>). The sensitivity analysis is performed to find the prominent reactions in the oxidation reaction mechanism. Based on the combustion characteristics, syngas HCCI maps are developed. The effect of engine operating conditions on combustion and emission characteristics is also investigated. Furthermore, the result of engine operating parameters on converting fuel energy into physical exergy, chemical exergy, work</p>

	exergy, and heat loss exergy is also briefly discussed.
28.	<p><a href="#">Explainable Supervised Domain Adaptation</a> V Kamakshi, NC Krishnan - International Joint Conference on Neural Networks (IJCNN), 2022</p> <p><b>Abstract:</b> Domain adaptation techniques have contributed to the success of deep learning. Leveraging knowledge from an auxiliary source domain for learning in labeled data-scarce target domain is fundamental to domain adaptation. While these techniques result in increasing accuracy, the adaptation process, particularly the knowledge leveraged from the source domain, remains unclear. This paper proposes an explainable by design supervised domain adaptation framework - XSDA-Net. We integrate a case-based reasoning mechanism into the XSDA-Net to explain the prediction of a test instance in terms of similar-looking regions in the source and target train images. We empirically demonstrate the utility of the proposed framework by curating the domain adaptation settings on datasets popularly known to exhibit part-based explainability.</p>
29.	<p><a href="#">FedDOVE: A Federated Deep Q-learning-based Offloading for Vehicular fog computing</a> V Sethi, S Pal - Future Generation Computer Systems, 2022</p> <p><b>Abstract:</b> Connected Autonomous Vehicles (CAVs) aim to provide various smart transportation applications which have computation-intensive tasks. The vehicles having less availability of computational resources offload tasks to roadside units (RSUs) for processing. Renewable energy-powered RSUs have limited energy, storage, and computational capabilities. To reduce the computation load at RSUs, vehicular fog computing is used for computation-intensive tasks. Vehicular fog computing brings the computational resources nearer to the requesting devices for reducing the latency in the request fulfillment. RSU computes the tasks either locally or offloads computation-intensive tasks to the fog server for further processing. In vehicular fog computing, one of the most important problems is to find an optimal association of RSUs with fog servers for computation offloading. A significant energy consumption occurs across RSUs in offloading computation-intensive tasks to fog servers. On the other hand, fog servers may have uneven computation load due to varying offloading rate across the road segments. The non-uniform distribution of computation load across fog servers may increase the latency in the request fulfillment. In this paper, we propose an online <b>Federated Deep Q-learning-based Offloading</b> technique for <b>Vehicular fog computing (FedDOVE)</b> which jointly optimizes the energy consumption across RSUs and load balancing across fog servers. FedDOVE is a model-free reinforcement learning approach that uses the global information for finding an optimal association between RSUs and fog servers. Simulation results show that the proposed FedDOVE reduces the energy consumption by about 47%–49% and improves load balancing by about 60%–65% as compared to other existing offloading techniques.</p>
30.	<p><a href="#">Finite Element Modeling and Experimental Validation of Tool Wear in Hot-Ultrasonic-Assisted Turning of Nimonic 90</a> J Airao, CK Nirala - Journal of Vibration Engineering &amp; Technologies, 2022</p> <p><b>Abstract:</b> Purpose</p> <p>Repetitive cutting nature of ultrasonic-assisted turning (UAT) has evidenced considerable enhancements in the machinability of difficult-to-cut materials. Pre-heating is another approach for improving the machinability of such materials. In this regard, a novel approach, combining ultrasonic vibration and pre-heating of a workpiece, is proposed to analyze the responses while cutting difficult-to-cut material. Thus, this study aims to develop a finite element (FE) model to estimate tool wear, chip–tool contact length and machining forces, under the combined effect, considering Nimonic 90 as workpiece material. The FE results are validated using an in-house developed setup.</p>

	<p><b>Methods</b></p> <p>The finite element model is developed for executing conventional turning (CT), UAT, and hot-UAT (HUAT) at 200 °C. The resonance frequency and amplitude used are 20 kHz and 10 µm, respectively, for the UAT and HUAT processes. Moreover, the horn is designed using FEM and fabricated to develop the UAT setup. The turning experiments of all three types are performed for Nimonic 90 under dry conditions at two different sets of process parameters. The induction heating technique is used for the HUAT to pre-heat the workpiece to maintain similar initial conditions as the FEM. The tool flank and crater wear, machining forces, and tool–chip contact length estimated by FEM are validated using the UAT setup.</p> <p><b>Results</b></p> <p>The results are examined in terms of tool flank and crater wear, tool–chip contact length, cutting force, and feed forces. The FEM and experimental results are found to be in close agreement with an approximate error of 2–25%. The main tool wear mechanisms detected are edge chipping, abrasion, adhesion of BUE, and fracture of tool nose. The HUAT reduces the tool–chip contact length by 5–21%, cutting force by 5–25%, and feed force by 14–36%, compared to CT and UAT. It is also observed that the error increases at the higher value of cutting speed. It is attributed to a catastrophic failure of the cutting edge at a higher cutting speed.</p> <p><b>Conclusion</b></p> <p>The HUAT and UAT show a substantial reduction in tool wear while machining at a low cutting speed. Whereas, at a higher cutting speed, the tool wear significantly increases in all three types of turning operations.</p>
31.	<p><a href="#">Finite Element Modeling of a Pressure Ulcers Preventive Bed for Neonates</a>  AN Mallick, M Kumar, K Arora, AK Sahani - IEEE-EMBS International Conference on Wearable and Implantable Body Sensor Networks (BSN), 2022</p> <p><b>Abstract:</b> The continual pressure on a skin surface can hamper blood supply from the subcutaneous regions. Blockage of blood supply is the primary reason for the development of Pressure Ulcers (PUs) in patients admitted to hospitals with impaired mobility. The dermal layer of a preterm neonate is less than 60% of the thickness of an adult and has a much higher susceptibility to developing pressure ulcers. In Neonatal Intensive Care Units (NICUs), babies lie down immobile for long hours in fixed positions. Hence, there is a 23% prevalence of PUs in NICUs worldwide. Therefore, it is advised that nursing staff should ensure frequent posture changes to avoid the development of PUs. This leads to an increased workload on them. We designed a Finite Element Modeling (FEM) of a neonatal anti-PU bed made from elastic material with alternating pressure channels and carried out simulations in ABAQUS CAE to validate this problem. We first simulated a neonatal phantom made from hyper-elastic material and laid it down on a flatbed. The pressure on the skin was taken as the baseline. We found that by activating alternating channels, the pressure increases in inflated regions and decreases in deflated regions compared to the baseline. As the inflation and deflation channels will be alternating, no long-term high-pressure points will be formed under the skin.</p>
32.	<p><a href="#">Fossil lizards and snakes (Diapsida, Squamata) from the Late Miocene hominid locality of Haritalyangar, India</a>  NP Singh, S Deep, A Čerňanský, RK Sehgal, AP Singh, N Kumar, P Uniyal, S Kumar... - Geobios, 2022</p> <p><b>Abstract:</b> The Late Miocene hominid-bearing locality in Haritalyangar, India, has yielded remains of fossil lizards and snakes. The material consists of the following taxa: <i>Varanus</i> and an</p>



	<p>indeterminate anguimorph, <i>Python</i>, a colubrid and a natricid. These squamates are documented from this region for the first time. A co-existence of <i>Varanus</i> and <i>Python</i>, two iconic squamates, is demonstrated. The overall fauna, which is dominated by both large and small semi-aquatic and terrestrial taxa, indicates seasonally wet sub-humid to semi-arid climate in the area during the Late Miocene, ~9.1 Ma. Moreover, the mean annual temperature must have been high in the region at that time (not less than 15–18.6 °C, similar to the mean annual temperature in this area today), indicated by the occurrence of important thermophilic elements such as <i>Varanus</i> and <i>Python</i>.</p>
33.	<p><a href="#">High entropy alloys (HEAs) as a binder material for heavy tungsten alloys, tungsten carbide hardmetals, and titanium carbo-nitride based cermet composites - a comprehensive review</a>  PK Katiyar, A Lavakumar, R Maurya, PK Singh - <i>Advances in Materials and Processing Technologies</i>, 2022</p> <p><b>Abstract:</b> The current review gives an insight into high-entropy alloys (HEAs) as a new possible binder material for the tungsten carbides, heavy tungsten alloys, and titanium carbo-nitride (Ti(C,N)) based cermet composites. The existing binder materials (for instance, Co, Ni, etc.), produced by powder metallurgy methods, have limited tool bits performance and short service life while mining applications; however, replacing existing binders with more accurate binder material is still a great challenge for researchers. Therefore, the present review is explicitly and precisely dedicated to the finding of the HEAs-based binder materials for the WC hard metals, heavy tungsten alloys, and Ti(C,N) cermet composites to produce high-performance drill bits associated with higher service life in the mining and cutting operations by improving the mechanical properties and tribo-corrosion performance. In this review, the performance of the HEAs over conventional binder materials has been compared and discussed concerning hardness, fracture toughness, oxidation, and tribo-corrosion resistance. The HEA-based binders showed low transformation kinetics and a lack of solubility as compared to the conventional binder. Hence, after optimising the composition, microstructures, properties, and costs of the HEAs-based binder materials, it can be estimated that in the upcoming year, the HEAs-based binder may replace the conventional binder.</p>
34.	<p><a href="#">Influence of competitive electro- and ferro-hydrodynamics on droplet vaporization phenomenology</a>  P Dhar, V Jaiswal, H Chate, LS Maganti - <i>Microfluidics and Nanofluidics</i>, 2022</p> <p><b>Abstract:</b> Modification and control of the vaporization kinetics of microfluidic droplets can find utilitarian implications in several scientific and technological applications. The article reports the control over the vaporization kinetics of pendant droplets under the influence of competing internal electrohydrodynamic and ferrohydrodynamic advection. Experimental and theoretical studies are performed and the morphing of vaporization kinetics of electrically conducting, paramagnetic fluid droplets using orthogonal electric and magnetic stimuli is explored. Analysis reveals that the electric field has a domineering influence compared to the magnetic field. While the magnetic field is observed to augment the vaporization rates, the electric field is observed to decelerate the same. Neither the vapour diffusion dominated model, nor the field induced modified surface tension characteristics can explain the observed behaviours. Velocimetry studies within the droplet show extensively modified internal ferro and electrohydrodynamic advection, which is noted to be the crux of the mechanism towards modified vaporization rates. A mathematical analysis is proposed, which takes into account the roles played by the concomitant governing Hartmann, Electrohydrodynamic, Interaction, thermal and solutal Marangoni, and the electro and magneto Prandtl and Schmidt numbers. It is observed that the morphing of the thermal and solutal Marangoni numbers by the electromagnetic Interaction number plays the dominant role towards morphing the advection dynamics. The model is able to predict the internal advection velocities accurately. The findings may hold importance towards smart control and tuning of vaporization kinetics in macro and microfluidic systems.</p>

35.	<p><a href="#">Influence of substrate roughness and ceramic content on deposition characteristics of cold-sprayed Ti/TiO<sub>2</sub> deposits</a>  A Kumar, H Singh, R Kant - <i>Metals and Materials International</i>, 2022</p> <p><b>Abstract:</b> Deposition of coatings on a cheaper substrate material is an economical, versatile, and effective way to enhance its surface properties and performance for the given application. Cold spray, a relatively new technology, has several advantages over other surface coating processes, including no phase change because of its low processing temperature. This work discusses the effects of substrate surface roughness and ceramic (TiO<sub>2</sub>) content in Ti-based feedstock powder on the coatings' deposition behavior. The results revealed that polishing the substrate to mirror-finish can be a better option for attaining good adhesion between the coatings and the substrate. Also, as the ceramic content increases in the feedstock, the deposition efficiency of the coatings affects severely and leads to poor mechanical properties. Finally, Ti/TiO<sub>2</sub> composite coatings have successfully been deposited and tested for corrosion and wear behavior. Cold sprayed Ti/20%TiO<sub>2</sub> composite coating is found to be successful in protecting the steel substrate from corrosion and wear.</p> <p><b>Graphical abstract:</b></p> 
36.	<p><a href="#">Natural rubber latex treatment of sand: A novel remediation technique for soil liquefaction</a>  U Veena, N James - <i>Soil Dynamics and Earthquake Engineering</i>, 2023</p> <p><b>Abstract:</b> We present a novel method to improve liquefaction resistance in sandy soil by treating it with natural rubber latex (NRL) using a pressurised permeation technique. Sand samples treated with NRL solutions of 10%, 15%, 20%, and 30% concentrations were tested. The liquefaction resistance of the untreated and NRL-treated sand samples was evaluated by performing strain-controlled cyclic triaxial tests with 0.15%, 0.3%, and 0.5% axial strain amplitudes. We find that NRL treatment reduces excess pore pressure development in the sand, thereby increasing liquefaction resistance. Further, this study also explores the effect of NRL treatment on stiffness deterioration in the sand under cyclic loading. NRL-treated sand samples showed resistance to progressive stiffness degradation even after many cycles due to interparticle bonding developed by virtue of the solidified NRL fibres. From a pilot study on the behaviour of treated sand under stress-controlled loading, it was seen that irrespective of the pore pressure development, NRL effectively resist the strain development in sand. Hence, we propose the utilisation of NRL as an environment-friendly soil stabiliser for mitigating liquefaction.</p>
37.	<p><a href="#">Non-trivial band topology in Bi doped Lanthanum monpnictides (LaX; X = As and Sb)</a>  P Wadhwa, TJD Kumar, A Shukla, R Kumar - <i>Solid State Communications</i>, 2022</p> <p><b>Abstract:</b> In this study, we report first-principles investigation of non-trivial topological characteristics in Bi doped Lanthanum monpnictides, particularly LaAs and LaSb. For this, we varied the concentration of Bi atoms in <math>1 \times 1 \times 2</math> supercell of LaAs and LaSb unit cells along [001] direction, and phonon-dispersion spectra of all these doped arrangements are observed to be dynamically stable. HSE06 band structure calculations with spin-orbit coupling reveal that the non-trivial topological characteristics starts appearing in 50% concentration of Bi atoms in the given supercells of LaAs and LaSb. The non-trivial topological characteristics in the proposed doped arrangements are verified by bulk band inversion, unit <math>Z_2</math> topological invariant, and a</p>

	<p>surface Dirac cone. Our findings provide promising candidates of non-trivial topological family, which may carry huge potential for extremely large magnetoresistance and spintronics applications.</p>
38.	<p><a href="#">Numerical assessment of a solar pond under transient state with realistic energy extraction from all possible zones</a> S Verma, R Das – Solar Energy, 2022</p> <p><b>Abstract:</b> A solar pond from which thermal energy is extracted from its non-convective zone (<i>NCZ</i>), lower convective zone (<i>LCZ</i>) and the ground below is modelled in transient state. The novelty of the study lies in the fact that heat extraction in each of the three zones is considered to be realistic, taking into account temperature drop across the exchanger surfaces. The pertinent weather parameters are described by curve fitting as series of sinusoidal time functions. Using these expressions, implicit finite difference method is used to solve the five coupled partial differential equations involved in the analysis, and the scaled down model is validated with simpler models available in the literature. To quantify the practical utility of pond, the final outgoing water stream heated from the pond is fed to a large scale solar still to assess the usefulness in a desalination application. Annual distillate production of the still coupled to such a pond is calculated and its variation with various manually adjustable parameters is studied. A total of 9 such parameters have been investigated. It is observed that there are five pond parameters related to pond's operation that possess optimum values that maximize annual distillate production. These are: <i>NCZ</i> and <i>LCZ</i> thicknesses, <i>NCZ</i> and <i>LCZ</i> exchanger pipes' radii, and ground extraction mass flow rate. An increase in any of the remaining parameters: upper convective zone (<i>UCZ</i>) thickness, ground exchanger pipes' radius and <i>NCZ</i>, <i>LCZ</i> extraction mass flow rates generate a decrease in distillate produced. It is also revealed that extraction should be carried from how many zones depends on the application coupled to the pond, and in this case, where the application is a solar still, <i>LCZ</i> with ground extraction turns out to be the best choice. Further, the assumption of ideal <i>NCZ</i> and ground extraction used in the literature is seen to overestimate system output by nearly 46%. Therefore, this model is a generalized one and various other single or dual zone extraction models available so far become subsets of it. This generalized model presented here can serve to design such a triple zone extraction based solar pond system in a realistic and practical manner and help evaluate suitable values of user-controlled variables that yield maximum output of the application to which the pond supplies energy.</p>
39.	<p><a href="#">On equilibrium solution to a singular coagulation equation with source and efflux</a> D Ghosh, J Paul, J Kumar - Journal of Computational and Applied Mathematics, 2022</p> <p><b>Abstract:</b> In this study, we analyze the existence of a steady-state solution to a coagulation equation with source and efflux for the following <i>singular</i> coagulation kernel: <math>K(x,y)=1+x^\lambda+y^\lambda(xy)\sigma</math>, where <math>0\leq\sigma\leq 12</math> and <math>0\leq\lambda-\sigma\leq 1</math>. The uniqueness of the steady-state solution is found in the space of functions which are continuous in <math>(0,\infty)</math>. Also, we find an explicit form of the equilibrium solution to the problem with sources and effluxes for the <i>constant</i> and <i>product</i> kernels; further, for a <i>linear</i> kernel, we provide a closed-form of the equilibrium solution. We provide a numerical example to support the proposed study.</p>
40.	<p><a href="#">Optimizing Trajectory and Dynamic Data Offloading Using a UAV Access Platform</a> A Kaur, SS Jha, J Jin, H Ghaderi - IoT, 2022</p> <p><b>Abstract:</b> The use of unmanned aerial vehicles (UAV) as an integrated sensing and communication platform is emerging for surveillance and tracking applications, especially in large infrastructure-deficient environments. In this study, we develop a multi-UAV system to collect data dynamically in a resource-constrained context. The proposed approach consists of an access platform called Access UAV (<i>A_UAV</i>) that stochastically coordinates the data collection from the Inspection-UAVs (<i>I_UAVs</i>) equipped with a visual sensor to relay the same to the</p>

	<p>cloud. Our approach jointly considers the trajectory optimization of A_UAV and the stability of the data queues at each UAV. In particular, the Distance and Access Latency Aware Trajectory (DLAT) optimization for A_UAVs is developed, which generates a fair access schedule for I_UAVs. Moreover, a Lyapunov-based online optimization ensures the system stability of the average queue backlogs for dynamic data collection while minimizing total system energy. Coordination between I_UAV and A_UAV is achieved through a message-based mechanism. The simulation results validate the performance of our proposed approach against several baselines under different parameter settings.</p>
41.	<p><a href="#">Oscillating Flow of Power-Law Fluids over a Sphere: Drag and Nusselt Number Behavior</a> G Mishra, RP Chhabra - <i>Chemical Engineering and Technology</i>, 2022</p> <p><b>Abstract:</b> The forced convection flow and heat transfer aspects of an isothermal sphere in an oscillating stream of power-law fluids in the range of <math>5 \leq Re \leq 120</math> and <math>0.3 \leq n \leq 1.5</math> are numerically investigated. The effects of shear-dependent viscosity and oscillatory flow features on the temporal variation of streamlines, patterns of streaming flows, drag coefficient, and Nusselt number are examined in depth. The power-law index modulates the transition of the steady streaming flows between two distinct streaming regimes. Overall, shear-thinning fluids at low oscillation frequencies are observed to yield significant increase in heat transfer. Due to the phase lag in the momentum boundary layer, the drag coefficient exhibits a phase lag ranging from <math>\pi/2</math> to <math>4\pi/5</math> whereas the Nusselt number lags by about 50 % of these values.</p>
42.	<p><a href="#">Performance Analysis of Evaporation and Heat Wheel-Based Building Air Conditioning Systems</a> G Singh, R Das - <i>Journal of Energy Resources Technology</i>, 2022</p> <p><b>Abstract:</b> Air conditioning in composite weather is relatively more challenging and also carries importance as it resembles conditions of hot-dry, cold, and warm-humid climates. Bifurcation of cooling and ventilation tasks happens to be one of the attractive techniques to design energy-efficient air-conditioning systems. It deals with the concept of providing a dedicated outdoor air system (DOAS) in conjunction with the air-conditioning unit. This study establishes the electrical energy consumption behavior of a building air-conditioning unit when modifications are done along the air pathway of the desiccant-integrated DOAS. For a 511 m<sup>2</sup> building situated in composite weather, simulations in energyplus are carried out after necessary validations with the available standards. Here, two modes are discussed: in the first one, an indirect evaporation cooler (IEC)-based system is analyzed, while in the second mode, a heat wheel has been studied. For regeneration, a solar collector and supplementary electrical heater are provided. For the dynamic pattern of site environmental conditions, variations of room air temperature, humidity, thermal load, electricity, thermal energy, and solar fraction have been studied. Current analysis demonstrates that approximately 2994 kWh of the total thermal energy delivered by solar collector and supplementary electrical heater system can be saved through heat wheel instead of IEC. The usage of a heat wheel in the airflow pathway of the desiccant-integrated DOAS can offer energy savings up to 5.04% of the electrical energy with respect to IEC-integrated DOAS. Furthermore, the suggested design delivers a higher solar fraction.</p>
43.	<p><a href="#">Physiological Sensing for Media Perception &amp; Activity Recognition</a> G Sharma - <i>Proceedings of the 2022 International Conference on Multimodal Interaction</i>, 2022</p> <p><b>Abstract:</b> Wearable sensors have the intriguing potential to continuously evaluate human physiological characteristics in real-time without being obtrusive. This thesis aims to incorporate physiological sensors data to investigate the Media Perception and Activity Recognition. Our primary research goals include (a) neural encoding-based psycho-acoustic attribute analysis for data sonification, (b) empirical evidence for perceptual subjectivity in neural encoding during human-media interactions, the impact of incorporating behavioral ratings, and (c) the efficacy of attention-based transformer models on physiological data on human activity recognition problems.</p>

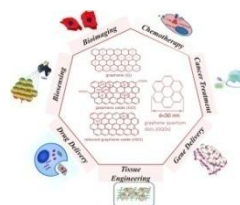
[Progress and challenges of graphene and its congeners for biomedical applications](#)

H Kaur, R Garg, S Singh... - Journal of Molecular Liquids, 2022

44.

**Abstract:** Nanomaterials by virtue of their small size and enhanced surface area, present unique physicochemical properties that enjoy widespread applications in bioengineering, biomedicine, biotechnology, disease diagnosis, and therapy. In recent years, graphene and its derivatives have attracted a great deal of attention in various applications, including photovoltaics, electronics, energy storage, catalysis, sensing, and biotechnology owing to their exceptional structural, optical, thermal, mechanical, and electrical. Graphene is a two-dimensional sheet of  $sp^2$  hybridized carbon atoms of atomic thickness, which are arranged in a honeycomb crystal lattice structure. Graphene derivatives are graphene oxide (GO) and reduced graphene oxide (rGO), which are highly oxidized and less oxidized forms of graphene, respectively. Another form of graphene is graphene quantum dots (GQDs), having a size of less than 20 nm. Contemporary graphene research focuses on using graphene nanomaterials for biomedical purposes as they have a large surface area for loading biomolecules and medicine and offer the potential for the conjugation of fluorescent dyes or quantum dots for bioimaging. The present review begins with the synthesis, purification, structure, and properties of graphene nanomaterials. Then, we focussed on the biomedical application of graphene nanomaterials with special emphasis on drug delivery, bioimaging, biosensing, tissue engineering, gene delivery, and chemotherapy. The implications of graphene nanomaterials on human health and the environment have also been summarized due to their exposure to their biomedical applications. This review is anticipated to offer useful existing understanding and inspire new concepts to advance secure and effective graphene nanomaterials-based biomedical devices.

**Graphical abstract:**



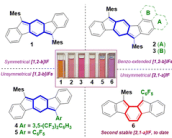
[Pseudo Decoder Guided Light-Weight Architecture for Image Inpainting](#)

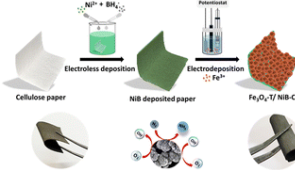
SS Phutke, S Murala - IEEE Transactions on Image Processing, 2022

45.

**Abstract:** Image inpainting is one of the most important and widely used approaches where input image is synthesized at the missing regions. This has various applications like undesired object removal, virtual garment shopping, etc. The methods used for image inpainting may use the knowledge of hole locations to effectively regenerate contents in an image. Existing image inpainting methods give astonishing results with coarse-to-fine architectures or with use of guided information like edges, structures, etc. The coarse-to-fine architectures require umpteen resources leading to high computation cost of the architecture. Other methods with edge or structural information depend on the available models to generate guiding information for inpainting. In this context, we have proposed computationally efficient, light-weight network for image inpainting with very less number of parameters (0.97M) and without any guided information. The proposed architecture consists of the multi-encoder level feature fusion module, pseudo decoder and regeneration decoder. The encoder multi level feature fusion module extracts relevant information from each of the encoder levels to merge structural and textural information from various receptive fields. This information is then processed with pseudo decoder followed by space depth correlation module to assist regeneration decoder for inpainting task. The experiments are performed with different types of masks and compared with the state-



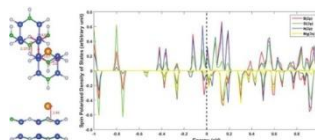
	<p>of-the-art methods on three benchmark datasets i.e., Paris Street View (PARIS_SV), Places2 and CelebA_HQ. Along with this, the proposed network is tested on high resolution images ( <math>1024 \times 1024</math> and <math>2048 \times 2048</math> ) and compared with the existing methods. The extensive comparison with state-of-the-art methods, computational complexity analysis, and ablation study prove the effectiveness of the proposed framework for image inpainting.</p>
46.	<p><a href="#">QoS-Aware Multipath Routing in Software-Defined Networks</a>  P Kamboj, S Pal, S Bera, S Misra - IEEE Transactions on Network Science and Engineering, 2022</p> <p><b>Abstract:</b> The emergence of new applications, such as online gaming and virtual reality, necessitates the underlying network capable of fulfilling high bandwidth and low latency requirements. The software-defined multipath routing is a viable approach to fulfill such quality-of-service (QoS) requirements by improving the data delivery performance through multipath. In this paper, we propose a QoS-aware dynamic multipath routing scheme for enhancing QoS of high-bandwidth applications in an SDN-enabled network. The proposed scheme consists of three phases – flow splitting, multipath routing, and flow reordering. In the first phase, we propose a flow splitting scheme to decide how to split the incoming flows to enable multipath routing in the network. In the second phase, we design a cost function for routing the splittable subflows and formulate a min-cost routing problem as an integer linear program (ILP). To solve the problem in polynomial time, we propose a greedy heuristic approach. Finally, in the third phase, we propose a flow reordering scheme for the received subflows through multiple paths to maintain the desired flow sequence at the destination. The experimental results show that the proposed scheme achieves higher network throughput by 22% compared to the benchmark schemes. Further, the proposed scheme achieves a reduction in QoS violated flows by 24% compared to the benchmark schemes.</p>
47.	<p><a href="#">Revisiting indeno[1,2-b]fluorene by steric promoted synthesis while isolating the second stable <math>4n\pi</math> indeno[2,1-a]fluorene</a>  H Sharma, N Bhardwaj, S Das - Organic &amp; Biomolecular Chemistry, 2022</p> <p><b>Abstract:</b> Described herein are the steric promoted synthesis and characterization of symmetric, unsymmetric, and benzo-extended indeno[1,2-<i>b</i>]fluorenes <b>1–5</b>, including the isolation of stable <math>4n\pi</math> indeno[2,1-<i>a</i>]fluorene <b>6</b>. Single-crystal XRD analyses of <b>5</b> and <b>6</b> gave the unambiguous confirmation of unsymmetrical [1,2-<i>b</i>]IF and [2,1-<i>a</i>]IF motifs, respectively. The different ground state antiaromaticity of <b>5</b> and <b>6</b> was explained by Gimarc's approach for topological charge destabilization. The electronic properties of unsymmetrical IFs <b>2–5</b> mostly lie midway between <b>1</b> and its other known symmetrical counterparts.</p> 
48.	<p><a href="#">Robust Unseen Video Understanding for Various Surveillance Environments</a>  P Patil, J Singh, P Hambarde, A Kulkarni, S Chaudhary, S Murala - IEEE International Conference on Advanced Video and Signal Based Surveillance (AVSS), 2022</p> <p><b>Abstract:</b> Automated video-based applications are a highly demanding technique from a security perspective, where detection of moving objects i.e., moving object segmentation (MOS) is performed. Therefore, we have proposed an effective solution with a spatio-temporal squeeze excitation mechanism (SqEm) based multi-level feature sharing encoder-decoder network for MOS. Here, the SqEm module is proposed to get prominent foreground edge information using spatio-temporal features. Further, a multi-level feature sharing residual decoder module is</p>

	<p>proposed with respective SqEm features and previous output features for accurate and consistent foreground segmentation. To handle the foreground or background class imbalance issue, we propose a region of interest-based edge loss. The extensive experimental analysis on three databases is conducted. Result analysis and ablation study proved the robustness of the proposed network for unseen video understanding over SOTA methods.</p>
49.	<p><a href="#">Self-standing Fe<sub>3</sub>O<sub>4</sub> decorated paper electrode as a binder-free trifunctional electrode for electrochemical ammonia synthesis and Zn-O<sub>2</sub> batteries</a>  A Kafle, D Gupta, A Bordoloi, TC Nagaiah – Nanoscale, 2022</p> <p><b>Abstract:</b> The conversion of the abundant biodegradable material into electroactive electrode material can be a good resource for sustainable energy conversion and storage applications. Herein, we present a simple, cost-effective and green approach for the fabrication of a flexible cellulose paper electrode using an electroless-electrodeposition method. The one-step electroless deposition route is followed to induce conductivity into a non-conductive cellulose paper substrate without using any expensive activators or sensitizers. The Fe<sub>3</sub>O<sub>4</sub> is then electrodeposited as an active catalyst over the conductive paper substrate for use in electrochemical activities. The as-fabricated paper electrode shows promising activity and stability during the dinitrogen reduction reaction (NRR) as well as oxygen bifunctional electrocatalysis. A faradaic efficiency of 4.32% with a yield rate of 245 <math>\mu\text{g h}^{-1} \text{mg}_{\text{cat}}^{-1}</math> at <math>-0.1 \text{ V}</math> is achieved for NRR whereas a very small overpotential of 180 mV is required to reach 10 <math>\text{mA cm}^{-2}</math> during OER, and the ORR reaction starts at the onset potential of 0.86 V. The practical applicability of the paper electrode is validated by assembling a Zn-O<sub>2</sub> battery showing a peak power density of 81 <math>\text{mW cm}^{-2}</math> and a stability up to 35 h during charge-discharge cycles, which can power the NRR to produce NH<sub>3</sub> under full cell conditions.</p> 
50.	<p><a href="#">Solar Powered Electric Drive-Train With Integrated Bidirectional DC/V2V Fast Charger Incorporating Switched Reluctance Motor</a>  V Shah, G Kumawat, S Payami - IEEE Global Conference on Computing, Power and Communication Technologies (GlobConPT), 2022</p> <p><b>Abstract:</b> The article proposes a solar-powered electric drive-train which integrates a bidirectional DC/vehicle-to-vehicle (V2V) fast charger incorporating switched reluctance motor (SRM) drive. The traction converter and phase windings are re-leveraged to charge the battery, thus eliminating the additional hardware required during charging. To extend the driving range, the charging and driving operation are simultaneously performed via the solar photovoltaic (PV) panel installed on the electric vehicle (EV) rooftop. When the EV is idle, the solar PV source installed on or external connects to the battery via the integrated bidirectional DC/V2V fast charger, which implements the maximum power point tracking (MPPT) algorithm. The integrated bidirectional DC/V2V fast charger also allows charging/discharging via another EV (EV2) battery source, commonly referred to as V2V charging. In addition, the proposed integrated drive-train (IDT) employs the same number of switches as with a standard n-phase asymmetric half-bridge converter and is also suitable for grid-to-vehicle (G2V), vehicle-to-grid (V2G) operation. Experiments on a prototype 1.1 kW SRM validate the effectiveness of the proposed drive-train, which supernumerary reduces the component footprint of the EV charging system.</p>
51.	<p><a href="#">Stacked Si2BN monolayers as ultra-high-capacity anode material for divalent Mg-ion batteries</a></p>

P Panigrahi, M Desai, R Ahuja, T Hussain – FlatChem, 2022

**Abstract:** In pursuit of developing next-generation energy storage systems, there has been increasing effort in multivalent rechargeable batteries, such as magnesium-ion batteries (MgIBs). Non-toxicity, earth abundance, and high storage capacity due to their divalent nature make MgIBs an ideal alternative to the existing lithium-ion batteries (LIBs). However, exploring efficient electrode materials capable of storing large quantities of Mg ions is one of the biggest challenges in actualizing MgIBs. Here first-principles density functional theory (DFT) simulations are employed to explore the potential of Si<sub>2</sub>BN monolayers as a novel anode material for MgIBs. We find that under the maximum coverage effect, the stacked Si<sub>2</sub>BN could attain a specific capacity of 359.94 mAh g<sup>-1</sup>, which further enhances to 1418.45 mAh g<sup>-1</sup> with a defect concentration of 12 %. The open-circuit voltages fall in the ranges of 0.42–0.46 V and 0.88–0.98 V for the pristine and defected Si<sub>2</sub>BN, respectively. Diffusion barrier calculations reveal that Mg ions diffuse 125 times faster on pristine Si<sub>2</sub>BN than the defected one. Our simulations determine that the electronic structures, binding mechanism, equilibrium cell voltages, ionic mobilities, and thermal stabilities of stacked Si<sub>2</sub>BN make it an excellent anode material for MgIBs.

**Graphical abstract:**



52.

[Supersolid-like solitons in two-dimensional nonmagnetic spin-orbit coupled spin-1 and spin-2 condensates](#)

P Kaur, S Gautam, SK Adhikari – Physics Letter A, 2022

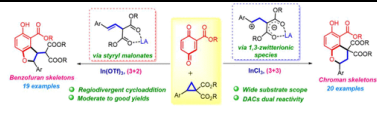
**Abstract:** We demonstrate spontaneous generation of spatially-periodic supersolid-like superlattice and stripe solitons in Rashba spin-orbit (SO) coupled spin-1 and spin-2 quasi-two-dimensional nonmagnetic Bose-Einstein condensates (BECs). The solitons in a weakly SO-coupled spin-1 BEC are circularly-symmetric of (−1,0,+1) and (0,+1,+2) types and have inherent vorticity; the numbers in the parentheses are the winding numbers in hyper-spin components +1,0,−1, respectively. The circularly-symmetric solitons in an SO-coupled spin-2 BEC are of types (−2,−1,0,+1,+2) and (−1,0,+1,+2,+3) with the former being the ground state, where the winding numbers correspond to spin components +2,+1,0,−1,−2, respectively. For stronger SO-coupling strengths, these solitons acquire a multiring structure while preserving the winding numbers. Quasi-degenerate stripe and super-lattice solitons, besides a circularly-asymmetric soliton, also emerge as excited stationary states for stronger SO-coupling strengths in spin-1 and spin-2 BECs.

53.

[Switchable Reactivity of Cyclopropane Diesters toward \(3 + 3\) and \(3 + 2\) Cycloadditions with Benzoquinone Esters](#)

N Kaur, P Kumar, A Hazra, P Banerjee – Organic Letters, 2022

**Abstract:** Herein, we describe an unprecedented (3 + 3) cycloaddition reaction of the donor–acceptor cyclopropanes with quinone esters toward the construction of chroman scaffolds in moderate to good yields. Interestingly, the strategy is also adjustable toward a (3 + 2) cycloaddition by just switching the Lewis acid to furnish benzofuran scaffolds. Based on the choice of Lewis acid used, the same set of precursors has been used to deliver the benzopyran and benzofuran derivatives.

	
54.	<p><a href="#">Synchrophasor Estimation: Review, Limitations and Future Trends</a>  M Pandit, R Sodhi - IEEE International Conference on Power Systems Technology (POWERCON), 2022</p> <p><b>Abstract:</b> This paper presents a state-of-the-art literature review on the existing synchrophasor estimation techniques, targeted to be used in Phasor Measurement Units (PMUs) in Wide Area Monitoring Systems (WAMS). Building upon the research gaps in the existing literature, the paper also highlights the latest trends and also, the future research directions in synchrophasor estimation.</p>
55.	<p><a href="#">Tailored light emission from color centers in nanodiamond using self-assembled photonic crystals</a>  S Sharma, Ashish, RV Nair - Frontiers in Nanotechnology, 2022</p> <p><b>Abstract:</b> The defect centers in solid-state materials especially the nitrogen-vacancy (NV) centers in diamond have shown a tremendous potential for their utilization in quantum technology applications. However, they exhibit certain drawbacks such as the feeble zero phonon line with huge phonon contribution and the higher lifetime values. Here, we present a novel approach to control the spontaneous emission from NV centers in nanodiamond using engineered self-assembled photonic crystals. Using two complimentary emission measuring geometries at room temperature, we show a 63% suppression and 17% enhancement of NV center emission intensity using photonic stopgap, supported with simulations. The emission rates are modified in a broad spectral range of NV center emission and are consistent with the Barnett–Loudon sum rule. The results are crucial for emerging quantum technologies using NV centers in diamond.</p>
56.	<p><a href="#">Targeting dendritic cells with TLR-2 ligand-coated nanoparticles loaded with Mycobacterium tuberculosis epitope induce antituberculosis immunity</a>  DK Das, MA Zafar, S Nanda, V Bhalla, JN Agrewala – Journal of Biological Chemistry, 2022</p> <p><b>Abstract:</b> Novel vaccination strategies are crucial to efficiently control tuberculosis, as proposed by the World Health Organization under its flagship program “End TB Strategy.” However, the emergence of drug-resistant strains of <i>Mycobacterium tuberculosis</i> (<i>Mtb</i>), particularly in those coinfecting with HIV-AIDS, constitutes a major impediment to achieving this goal. We report here a novel vaccination strategy that involves synthesizing a formulation of an immunodominant peptide derived from the Acr1 protein of <i>Mtb</i>. This nanoformulation in addition displayed on the surface a toll-like receptor-2 ligand to offer to target dendritic cells (DCs). Our results showed an efficient uptake of such a concoction by DCs in a predominantly toll-like receptor-2-dependent pathway. These DCs produced elevated levels of nitric oxide, proinflammatory cytokines interleukin-6, interleukin-12, and tumor necrosis factor-<math>\alpha</math>, and upregulated the surface expression of major histocompatibility complex class II molecules as well as costimulatory molecules such as CD80 and CD86. Animals injected with such a vaccine mounted a significantly higher response of effector and memory Th1 cells and Th17 cells. Furthermore, we noticed a reduction in the bacterial load in the lungs of animals challenged with aerosolized live <i>Mtb</i>. Therefore, our findings indicated that the described vaccine triggered protective anti-<i>Mtb</i> immunity to control the tuberculosis infection.</p>

**Disclaimer:** This publication digest may not contain all the papers published. Library has compiled the publication data as per the alerts received from Scopus and Google Scholar for the affiliation “Indian Institute of Technology Ropar” for the month of November 2022. The author(s) are requested to share their missing paper(s) details if any, for inclusion in the next publication digest.